A CIRCUIT FOR THE CONTROL OF IONIZING CURRENT BY A SATURABLE CORE TRANSFORMER

By B. M. BANERJEE * and AMBUJ MUKERJEE

(*Received for publication, April 30, 1917*)

ABSTRACT A simpler version of the Overbeck Meyer circuit for automatic control of ionizing current is described. A mathematical analysis for the circuit is presented. Theoretical calculations in a practical case are checked against experimental observations.

The discovery of a simple and interesting relation between A. C. permeability and D. C. magnetizing current is reported.

A new phenomenon—self oscillation of the D. C. current in such a circuit is reported. An explanation about the mechanism of such oscillations is also suggested.

The design of this circuit is discussed in detail. A step by step method of design outlined.

Finally the advantages and disadvantages of this type of circuit is compared with other types of control circuits.

INTRODUCTION

In devices † where a stream of electrons are used to ionize a gas, the necessity of keeping this ionizing current constant, frequently arises. The ionizing current in such devices is inherently unstable, being greatly dependent on the gas pressure and the surface conditions of the electron emitting filament. Means must therefore be provided for continuous adjustment of the filament current so as to compensate for, by altering the filament temperature, the effects of cumulative ionization at high pressures and of surface activation and poisoning with different types of gases. Many circuits have been proposed. We give below another. This is a simplified version of the Overbeck and Meyer (1934) circuit. This circuit, like the Overbeck and Meyer circuit, is primarily meant for use with ionization gauges although it may be used in any of the other devices mentioned below with suitable modification.

Circuit.

The circuit diagram is given below. It will be seen that here we have only a series resonating capacity in place of the series inductance and parallel resonating capacity of the Overbeck Meyer circuit. From the circuit point of view both circuits are intrinsically the same as both lead effectively to the same equivalent circuit which is analysed below :

* Fellow of the Indian Physical Society.

† (1) Ionization gauge, (2) Ion tubes and sources, (3) Mass spectrometer, -

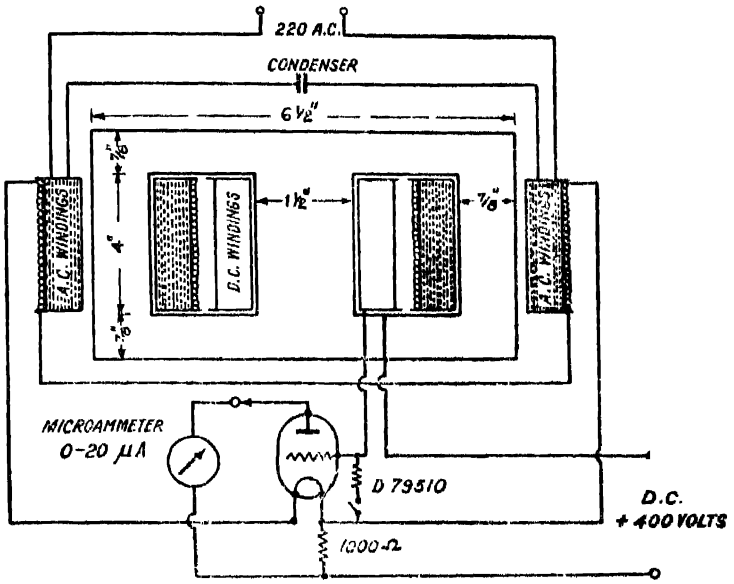

FIG. 1

Saturable Core transformer and control circuit.

Details of saturable core transformer: Core of .20 S.W.G. transformer sheets; core thickness 1½"; Two a.c. windings on two outer limbs; Primary: (3500+3500) turns of No. 30 S.W.G. enamelled wire, total d.c. resistance 220 ohms insulating paper between layer to layer. Secondary: (20+15)+(20+15) turns of No. 16 S.W.G. D.C.C. wire wound in a single layer above the primary winding, three layers of empire cloth insulation between primary and secondary. D.C. winding on central limb, 50,000 turns of No. 42 S.W.G. enamelled wire, total resistance 20,000 ohms, no insulating paper between layer to layer. All formers made with thick presspahn paper.

Ion gauge tube is a Western Electric D79510 tube.

For reactivation of the oxide coated filament of this gauge, the resistance between the grid and filament may be switched on. A current will then pass through the d.c. winding and a maximum filament voltage will be developed and maintained across the filament so long as the emission does not appear. Appearance of emission will be accompanied by an automatic reduction in the filament voltage and the switch may be thrown off to get the normal stabilized value (10.5 m.A) of the emission current.

Analysis: The mode of operation of the circuit may be understood from an analysis of the equivalent circuit.

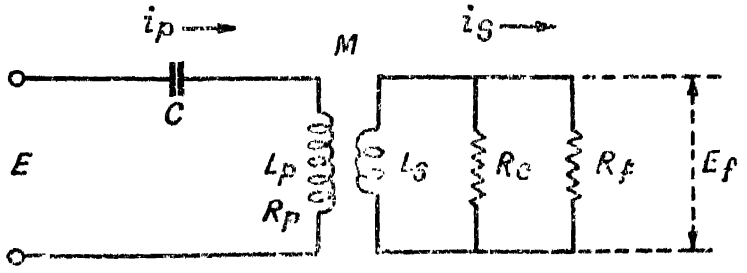

FIG. 2

Fig. 2. Equivalent Electrical Circuit. R_p = D. C. resistance of the A. C. windings. R_f = Resistance of the ion tube filament and the resistance of the secondary windings; R_e = Resistance coming about due to eddy current losses in the core.

The voltage induced in the secondary windings is given by the relation

$$E_s = jpMi_p \qquad \ldots (1)$$

And
$$i_p = \frac{E}{-1/pc + jpL_p + R_p + \left(\frac{p^2M^2}{R_s^2 + p^2L_s^2}\right)R_s - jpL_s\left(\frac{p^2M^2}{R_s^2 + p^2L_s^2}\right)} \qquad (2)$$

where $R_s = \dfrac{R_e R_f}{R_e + R_f}$. $\qquad \ldots (3)$

Now $L_p = \dfrac{4\pi n_1^2 A\mu}{l.10^9}$ Henries :

$M = \dfrac{4\pi n_1 n_2 A\mu}{l.10^9}$,,

$L_s = \dfrac{4\pi n_2^2 A\mu}{l.10^9}$,,

and turns ratio

$$T = \frac{n_1}{n_2}.$$

n_1 = Primary turns.

n_2 = Secondary turns.

A = Area of cross section of the core.

μ = A. C. permeability.

l = length of A. C. flux path in core.

Putting $\alpha = \dfrac{4\pi n_2^2 A}{l.10^9}$, we get

$$\left.\begin{aligned} L_s &= \alpha\mu \\ M &= \alpha T\mu \\ L_p &= \alpha T^2\mu. \end{aligned}\right\} \qquad \ldots (4)$$

Also putting $R_s = (k/\mu)$ $pL_s = kp\alpha$
and remembering $M^2 = L_p L_s$ and $T^2 = L_p/L_s$
we obtain from (1) and (2)

$$|E_s| = \frac{p\alpha TE\mu}{\left[\left\{\left(\frac{k^2/\mu^2}{k^2/\mu^2+1}\right)p\alpha T^2\mu - \frac{1}{pc}\right\}^2 + \left\{R_p + \frac{T^2R_s}{k^2/\mu^2+1}\right\}^2\right]^{\frac{1}{2}}}$$

whence

$$|i_s| = \frac{p\alpha TE\mu}{\left[\left\{\left(\frac{k^2/\mu^2}{k^2/\mu^2+1}\right)p\alpha T^2\mu - \frac{1}{pc}\right\}^2 + \left\{R_p + \frac{T^2R_s}{k^2/\mu^2+1}\right\}^2\right]^{\frac{1}{2}}\left[R_s^2 + p^2\alpha^2\mu^2\right]^{\frac{1}{2}}}$$

and
$$E_f = \frac{p\alpha TE\mu.R_s}{\left[\left\{\left(\frac{k^2/\mu^2}{k^2/\mu^2+1}\right)p\alpha T^2\mu - \frac{1}{pc}\right\}^2 + \left\{R_p + \frac{T^2R_s}{k^2/\mu^2+1}\right\}^2\right]^{\frac{1}{2}}\left[R_s^2 + p^2\alpha^2\mu^2\right]^{\frac{1}{2}}} \qquad \ldots (5)$$

E_f is the ion gauge tube filament voltage.

DISCUSSION ON RESULTS OF ANALYSIS AND EXPERIMENT

Equation (5) expresses E_f as a function of μ, the A. C. permeability. As is well known, the A. C. permeability of the iron core changes with D. C. magnetisation. The D. C. magnetisation of the transformer core is caused by the ionizing current of the ion gauge tube which passes through the D. C. winding on the central limb of the transformer. Thus a change in the ionizing current will cause a change in the A. C. permeability of core and hence a change in the filament voltage. In other words the filament voltage will be a function of the ionizing current as it is a function of μ.

A set of five theoretical curves will be found in Fig. 3. These represent Eq. (5)— filament voltage as a function of μ — the A. C. permeability. The ordinates in the curves of Fig. 3 are drawn proportional to $1/\mu$. The curves are for a transformer of the dimensions given in Fig. 1.

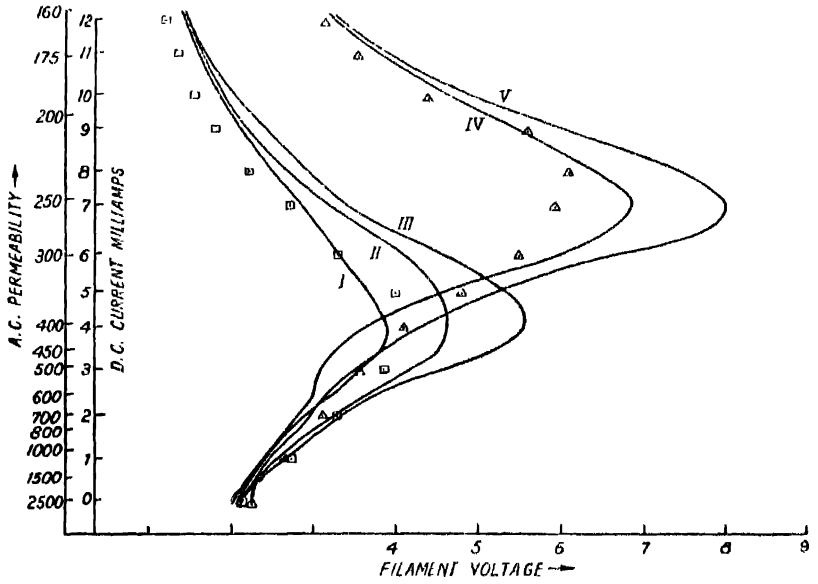

FIG. 3

Theoretical curves for a saturable core transformer of the dimensions given in Fig. 1. All the curves are for a turns ratio of 100 (Primary = 7000 turns, Secondary = 70 turns). Filament voltage plotted is 90% of that given by equation (5) to allow for the drop in the resistance and leakage inductance of the secondary.

curve I, $c = .33\mu f$;	$R = 2.0$ ohm
curve II, $c = .33\mu f$;	$R = 2.5$ ohm.
curve III, $c = .33\mu f$;	$R = 3.0$ ohm
curve IV, $c = \frac{1}{2}\mu f$;	$R = 2.5$ ohm.
curve V, $c = \frac{1}{2}\mu f$;	$R = 3.0$ ohm.

The squares are the experimental points for $c = .33\mu f$. The triangles are the experimental points for $c = \frac{1}{2}\mu f$. Secondary load D795/0 tube. This tube takes 1.4 amps at 3.4 volts and 2.2 amps at 7.5 volts on the filament.

The curves were drawn as a function of $1/\mu$, rather than μ, because it was found that μ — the A. C. permeability (at constant A. C. flux density in the core) varies with the D. C. magnetizing current (*i.e.*, the D. C. magnetization)

such that the relation between $1/\mu$ and the D. C. magnetizing current is almost a straight line. See curves in Fig. 4. This interesting relation appears not to have been observed or reported to previously by any other worker. The relation means that the admittance of an iron cored reactor increases linearly with the D. C. magnetization. The simplicity of the relation makes it important.

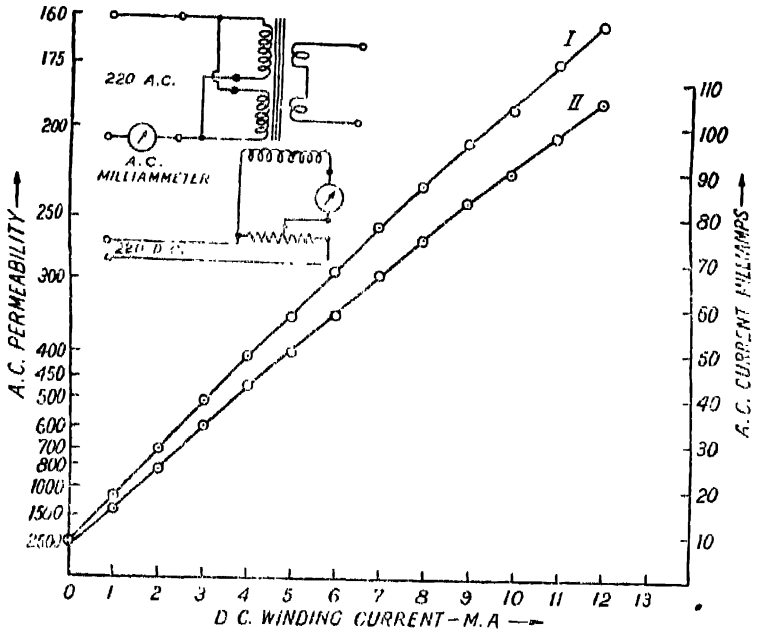

FIG. 4

A.C. permeability at constant flux density vs D.C. magnetization curve I. The ordinates in curve I are proportional to $1/\mu$. The A.C. flux density in the core was approximately 4000 gauss. The d.c. magnetization would amount to 1.7 gilberts per cm per milliampere if leakage were neglected. It will be observed that an almost linear relation exists between $1/\mu$ and D.C. magnetization. This discovery will be of great help in future designs of reactors and transformers where a D.C. magnetization takes place. (A.C. current in curve II is half the total current).

A set of four experimental curves—filament voltage vs. D. C. winding current—are given in Fig. 5. They have the same general nature as the theoretical curves in Fig. 5. The experimental points of the curves I and II are also plotted in Fig. 3. as small triangles and squares. It will be appreciated that the experimental points correspond to a curve for a secondary resistance lying between 2 and 2.5 ohms. The agreement between the theoretical and experimental values is good. The discrepancy that is observed is due to the following reasons :—

(1) The filament resistance is a variable one in the experimental case. The resistance of the ion-gauge tube filament varies with temperature. So it is smaller for a smaller voltage and greater for a larger one. The filament voltage in the experimental curves may therefore be expected to drop off more sharply and down to lower values than predicted by the theoretical curves.

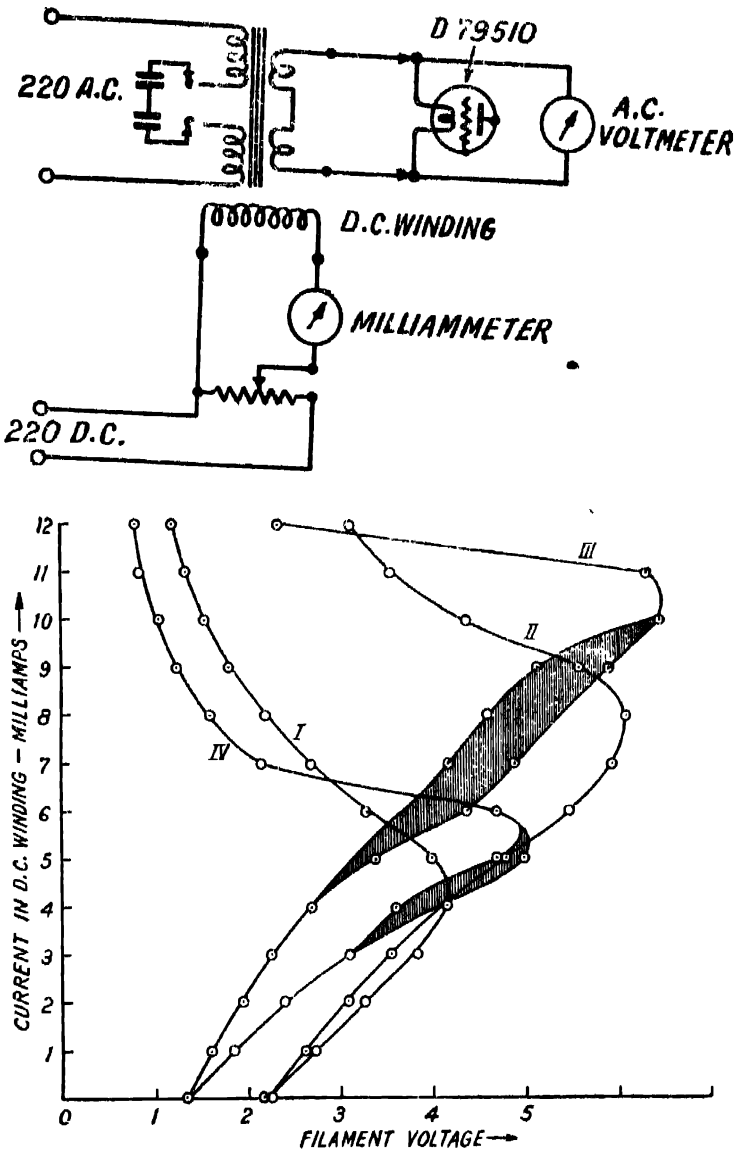

FIG. 5

Experimental curves for a saturable core transformer control circuit. Circuit, Ion gauge tube and transformer data given in Fig 1,

Curve I—for $c = \frac{1}{4}\mu f$, secondary turns 70
Curve II—for $c = \frac{1}{2}\mu f$, secondary turns = 70
Curve III—for $c = \frac{1}{2}\mu f$; secondary turns = 50
Curve IV—for $c = \frac{1}{2}\mu f$; secondary turns = 40

In the circuit of Fig. 1 with the constants for curve III, the stabilized value of the current is near about 10 5 m.A. With the constants of curve IV, the stabilized current is about 6 M.A. So, if it is desired to change the operating current of the ion-gauge tube, the resonating capacity may be changed to achieve this over a limited range. Shaded area in curves III and IV represent regions of oscillation.

(2) In the experimental case the A. C. permeability drops off beyond the resonance point by virtue of two causes

(*a*) the increasing D. C. magnetization.

(*b*) the reducing A. C. magnetization.

The latter is not taken into account in fixing the points for the experimental curves. Hence the experimental values of voltage are found to be smaller than the calculated ones for they actually correspond to lower values of μ.

(3) The effect of magnetic leakage is not taken into account in the calculations. As leakage increases with decrease of μ, the voltages observed are smaller than the calculated ones, in the region where μ is small.

STABILIZATION OF IONIZING CURRENT

The device will stabilize the ionizing current flowing also through the D. C. winding in the region where the secondary voltage decreases with increase of D. C. winding current. For, an increase in the ionizing current will also result in an increase of the D. C. winding current which will produce a decrease in the secondary voltage and thus the filament temperature and emission and *vice versa*. Thus a tendency of a change in the ionizing current will be suppressed. The stable point is given by the intersection of the filament voltage—emission current curve of the ion gauge tube with the secondary voltage—saturating current curve of the saturable core transformer circuit. Changes in the ionizing current may take place due to changes in pressure and composition of the gas in the ion-gauge tube and due to line voltage fluctuations. These will respectively modify the filament voltage—emission current curve of the ion gauge tube and the D. C. current—secondary voltage curve of the saturable core transformer circuit and so alter the stable point.

The stabilizing control will be more efficient if the slope of the secondary voltage—D. C. winding current be steep. Thus the control becomes increasingly efficient as we pass on to curves I, II, IV, III in order. It will be noticed from the theoretical as well as the experimental curves, that the slope is greater and stabilizing action more powerful for,

(*a*) a secondary load of higher resistance.

(*b*) a series capacity of $\cdot 5\mu f$ — which resonates the transformer at a permeability of 250-300.

(*c*) for a higher turns ratio.

Oscillation.—The experimental curves III and IV show that there is a region of oscillation—the D. C. winding current and the filament voltage (in the circuit of Fig. 5) oscillating at a frequency lying between 40 to 100 cycles per minute. Such a phenomenon was not reported by Overbeck and Meyer. It appears to be quite a common phenomenon when the resonance is sharp. It can be explained away in the following way :—

A. C. permeability depends on D. C. winding current ; A. C. permeability also depend on A. C. magnetization.

Further,

D. c. Flux density depends on D. C. winding current ; D. C. Flux density also depend on A. C. magnetization.

Thus a change in D. C. winding current will produce a change in A. C. permeability and a change in A. C. winding current and so a change in A. C. magnetization. The change in A. C. magnetization, will produce a change in D C. flux density, which may reinforce the original change in the D. C. winding current, and result in an oscillation of the D. C. winding current and an osciilation of the amplitude of the secondary voltage.

The period of oscillation will depend on :—

(*a*) Time taken for the establishment of a change in the A. C. winding current and consequent change in A. C. magnetization. In the resonant circuit formed by the A. C. winding with the capacity C some time must elapse before the current can alter its magnitude. This time is of the order of a fraction of a second.

(*b*) Time taken for the establishment of the current in the D. C. winding. This depends upon the time constant of the D. C. winding. This is also a fraction of a second.

The overall period is the sum of the two. It was found to lie between half a second to one and a half seconds depending upon whether load was connected to the secondary or not. This fits in well with what may be expected. The correctness of the explanation was further verified by putting a resistance in series with the D. C. winding. This shortened the time period as expected.

DESIGN OF THE TRANSFORMER

It was pointed out earlier that the stabilizing action becomes more perfect,

(*a*) with a secondary load of higher resistance,

(*b*) for a greater turns ratio, T,

(*c*) for a resonating permeability lying between 250-400.

The secondary load will have a higher resistance value if the eddy current losses are minimized. This may be achieved by using thin laminations of high specific resistance transformer sheets to form the core. Wooden core clamps should be used to eliminate eddy current losses in the clamps and also to reduce leakage of D. C. and A. C. magnetic flux. Leakage of both D. C. and A. C. flux lines tend to reduce the efficiency of control.

The turns ratio T cannot be increased indefinitely. With a greater value the secondary voltage will be smaller. Most useful design results when the maximum secondary voltage of the secondary voltage—D. C. winding current curve of the circuit coincides with the maximum rating of the ion gauge tube.

The capacity value chosen should be sufficiently large so that *resonance is possible, i.e.*, the reactive volt-amperes be several times (at least three) greater than the filament power. The dimensions of the transformer core should be big enough to secure the resonance inductance at a permeability

not smaller than 250, otherwise the system will fail to give satisfactory stabilizing action.

The D. C. winding should have sufficient number of turns to reduce the A. C. permeability to values below the resonance permeability.

A method of step by step design of the transformer is outlined below :

1. Find out the maximum filament power (w) required by the ion-gauge tube.

2. Set upon a suitable value Q, for the ratio reactive volt amperes (W) to filament power (w). It should have a value not less than three for good stabilizing action.

3. The maximum voltage across the series capacity will then be approximately Q times the supply voltage. Calculate the capacity from the relation,

$$(QE)^2 p.c. = Q.w$$

4. The maximum primary voltage is also QE approximately. The maximum secondary voltage is to be equal to the maximum rating of the ion-gauge tube. So

$$\text{Turns ratio} = \frac{Q.E.}{\text{Max. rated ion tube filament voltage}}$$

5. Calculate the size of the transformer from the relations

$$W = \tfrac{1}{2} p L_1 I^2$$

and

$$\tfrac{1}{2} L_1 I^2 = VB^2/8\pi\mu$$

where B is the flux density, μ the A. C. permeability and V the volume of iron in the A. C. limbs of the core.

So that

$$W = pVB^2/8\pi\mu$$

whence

$$V = W.8\pi\mu/pB^2 = 8Qw\pi\mu/pB^2$$

This sets the volume of iron in the A.C. limbs of the core and thus the size of the transformer.

V increases and so the size becomes greater as

(*a*) w—the filament power increases

(*b*) Q increases.

Since control becomes more efficient with higher values of Q, *efficient control means increased size.*

Smaller size results when the resonating permeability is small and B is large. But as has been remarked earlier, it is not practical to use μ values less than 250 and B greater than 10,000 gauss.

6. Calculate the number of turns required in the primary and secondary for the dimensions of the core (calculated in step 5) from the relations

(*a*) volts per turn $= \dfrac{4.44 \ B.A.f.}{10^8}$

where B = Maximum flux density in core.

A = Area of cross section of core.

f = supply frequency.

(*b*) Maximum primary voltage—Q. E.

(*c*) Maximum secondary voltage = Maximum rated ion tube voltage.

7. From the wire tables select suitable wire sizes for the primary and secondary. The maximum secondary current is equal to the maximum rating of the gauge tube filament. The maximum primary current is obtained from the relation

Maximum primary current = Q. E. p. c.

8. The D. C. winding of the transformer should be put on the central limb. This eliminates A. C. voltages from the D. C. turns. The central limb should have an area of cross-section approximately twice the outer A. C. limbs.

From the wire tables select the wire size for the D. C. winding. The current it has to pass is equal to the ionizing current of the ion-gauge tube. Calculate the number of turns that may be put in the space available. Hence calculate the resistance of the winding and also the D. C. voltage drop across it If this is excessive a thicker gauge must be used.

Steps 6, 7 and also 8 may point towards an increased size for the transformer. In that case the calculations are to be repeated assuming a greater value of resonance μ in step 5.

PERFORMANCE

The performance of an actual circuit is described in the curves of Fig. 5. The curves themselves cannot give an exact idea of the actual stabilization obtained against line voltage fluctuations and gas pressure variations. The variation of the ionizing current with line voltage fluctuations and gas pressure variations were therefore separately studied and the results are as follows :

1. For a change of line voltage from 226 volts to 240 volts, the change in the ionizing current was only 0.5 m. A. in 10.5 m. A. This variation of line voltage affected both the saturable core transformer circuit as well as the rectified D. C. supply for the ionizing current.

2. Change in the ionizing current was not discernible for gas pressure changes from the "blue glow" region (pressure higher than 10^{-3} mm.) to lower than 10^{-4} mm. However, the filament voltage dropped and glow of the filament disappeared as the vacuum worsened from 10^{-4} mm. to the "blue glow" region.

CONCLUSION

The circuits that appear to be generally adopted as a control circuit of ionizing current is some variation of the circuit described by Ridenour and Lampson (1937). This circuit uses many valves and components. The

The second division in the region 4800-2370A consists of diffuse bands which apparently occur in groups except for the continuum at 3416A and three other broad bands at 4747, 4662 and 4575A, which may also be regarded as continua (*vide* Papers I, II and III). These groups of diffuse bands, together with the continua can be explained as arising in stable states and having for their final levels different repulsive states. In general, the constituent bands of different groups are well separated from one another with wavenumber differences which approximately agree with the vibrational frequencies of the stable states that form the initial levels of these groups. The different stable states which are involved in giving rise to the bands in the region 4800 to 2370A are σ_g, π_u^4, π_g^4, σ_u. $1_u^+ (^3\Sigma_u^+)$; σ_g, π_u^4, π_g^3, σ_u^2. $1_g(^3\Pi_{1g})$; σ_g, π_u^4, π_g^3, σ_u. $0_u^+(^1\Sigma_u^+)$; σ_g, π_u^4, π_g^3, σ_u^2. $1_g(^1\Pi_g)$ and $\{(\sigma_g^2, \pi_u^4, \pi_g^3. {}^2\Pi_{\frac{3}{2}g})\sigma_g^x\}\Pi_{2,1g}$ at 44900, 51528, 51683, 58572 and 56000 cm^{-1} with ω values 90, 215, 165, 120 and 360 cm^{-1} respectively (*vide* Fig. 1). Of these the first and the third are observed in absorption as forming the final levels of the Pringsheim-Rosen, Kimura-Miyanishi (P-R, K-M) bands between 2760-1950A (Paper VII) and Cordes bands (Paper VI) in the fluorite region 1950-1770A respectively. The other three states cannot combine with the ground state σ_g, π_u^4, π_g^4; 0_g^+ $(^1\Sigma_g^+)$ because of the $g \leftarrow\!\!\!\!\rightarrow g$ rule, and as such they are not observed in absorption.

There are five groups with wavenumber differences of the order of 165 cm^{-1} among the constituent bands, which arise in the state 0_u^+ $(^1\Sigma_u^+)$ at 51683 cm^{-1} with $\omega = 165.1$ cm^{-1} (Paper I). These five groups have for their final levels the following repulsive state: 0_g^+ $(^1\Sigma_g^+)$, 0_g^+ $(^3\Sigma_g^-)$, 1_g $(^3\Sigma_g^-)$, $1_g(^1\Pi_g)$ and 0_g^+ $(^3\Pi_{0_g^+}$(of which the first dissociates into $I(^2P_{\frac{1}{2}}) + I(^2P_{\frac{1}{2}})$ atoms at 27637 cm^{-1}; the second, third and fourth into $I(^2P_{\frac{3}{2}}) + I(^2P_{\frac{1}{2}})$ atoms at 20037 cm^{-1} and the fifth into $I(^2P_{\frac{3}{2}}) + I(^2P_{\frac{3}{2}})$ at 12437 cm^{-1}, (*vide* Fig. 1).

Five groups with a wavenumber separation of about 215 cm^{-1} among the constituent bands (Paper II), arise in the state 1_g $(^3\Pi_{1g})$ with $\omega \backsim 215$ cm^{-1} at 51528 cm^{-1}. They have for their final levels the following repulsive states: $1_u(^3\Sigma_u^+)$, $0_u^-(^3\Sigma_u^+)$, $1_u(^3\Delta_{1u})$, $2_u(^3\Delta_{2u})$ and $1_u(^1\Pi_u)$ of which the first two dissociate into two $I(^2P_{\frac{1}{2}})$ atoms, and the remaining into $I(^2P_{\frac{3}{2}}) + I(^2P_{\frac{1}{2}})$ atoms. The state $\Pi_{2,1g}$ forms the initial state of the five groups of bands with a wavenumber separation of the order of 360 cm^{-1} among the constituent bands. The final levels of these groups are the same as those of the groups arising in the $1_g(^3\Pi_{1g})$ state. The state $1_g(^1\Pi_g)$ at 58572 cm^{-1} with $\omega \backsim 120$ cm^{-1} forms the initial level of three groups of bands from 2685-2448A which have for their final levels the same repulsive states as the last three groups arising in $1_g(^3\Pi_{1g})$ and $\Pi_{2,1g}$ (Paper III). Between 2500-2370A there are some bands which are difficult to be measured and some of which may be extensions of the three groups of bands arising in $1_g(^1\Pi_g)$

and others may be due to the transitions which are theoretically possible, notably $O_u^+ (^1\Sigma_u^+) \rightarrow 1_g(^3\Pi_{1g})$; $1_g(^3\Pi_{1g}) \rightarrow 1_u(^3\Pi_{1u})$ and $1_u(^3\Pi_{1g}) \rightarrow O_u^- (^3\Pi_{0-})$, where the three final levels dissociate into two $I(^2P_{\frac{3}{2}})$ atoms. (See Table III and Fig. 1).

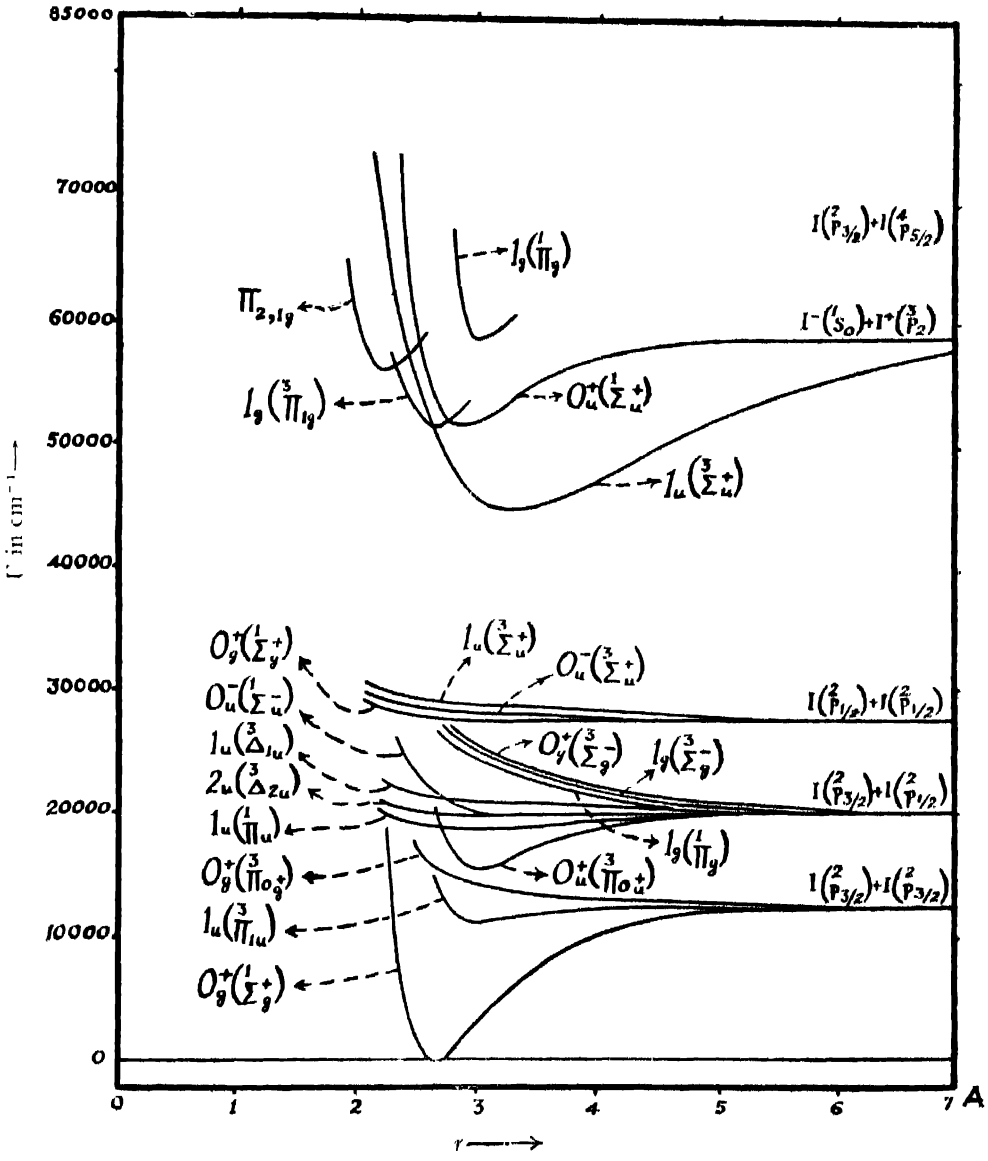

FIG. 1

Potential energy curves for I_2 molecule

Of all the various transitions, the following determine the coupling for iodine molecule as of case (*c*) type :

(1) $O_u^+ (^1\Sigma_u^+) \rightarrow O_g^+ (^3\Sigma_g^-)$; (3) $1_u (^3\Sigma_u^+) \rightarrow O_g^+ (^3\Sigma_g^-)$

(2) $O_u^+ (^1\Sigma_u^+) \rightarrow 1_g (^3\Sigma_g^-)$; (4) $1_u (^3\Sigma_u^+) \rightarrow 1_g (^3\Sigma_g^-)$.

Of these the first two represent the second and third groups arising in the state O_u^+ ($^1\Sigma_u^+$) (Paper I) and the remaining two represent the two broad bands at 4747, 4662A arising in 1_u ($^3\Sigma_u^+$) (Paper III). These transitions would not have been possible if the coupling is case (*a*) or (*b*) type, because of $\Sigma^+ \leftarrow\!|\!\rightarrow \Sigma^-$ rule. The fact that these transitions are present is a clear proof of the existence of case (*c*) type coupling in these states of iodine. All the other transitions will be possible for case (*c*) type coupling as well as case (*a*) or (*b*) type coupling provided the singlet$\leftarrow\!|\!\rightarrow$triplet rule is not strict.

(2) *Bromine* : The spectrum of bromine, as that of iodine can also be divided broadly into two divisions (Paper IV). The first division between

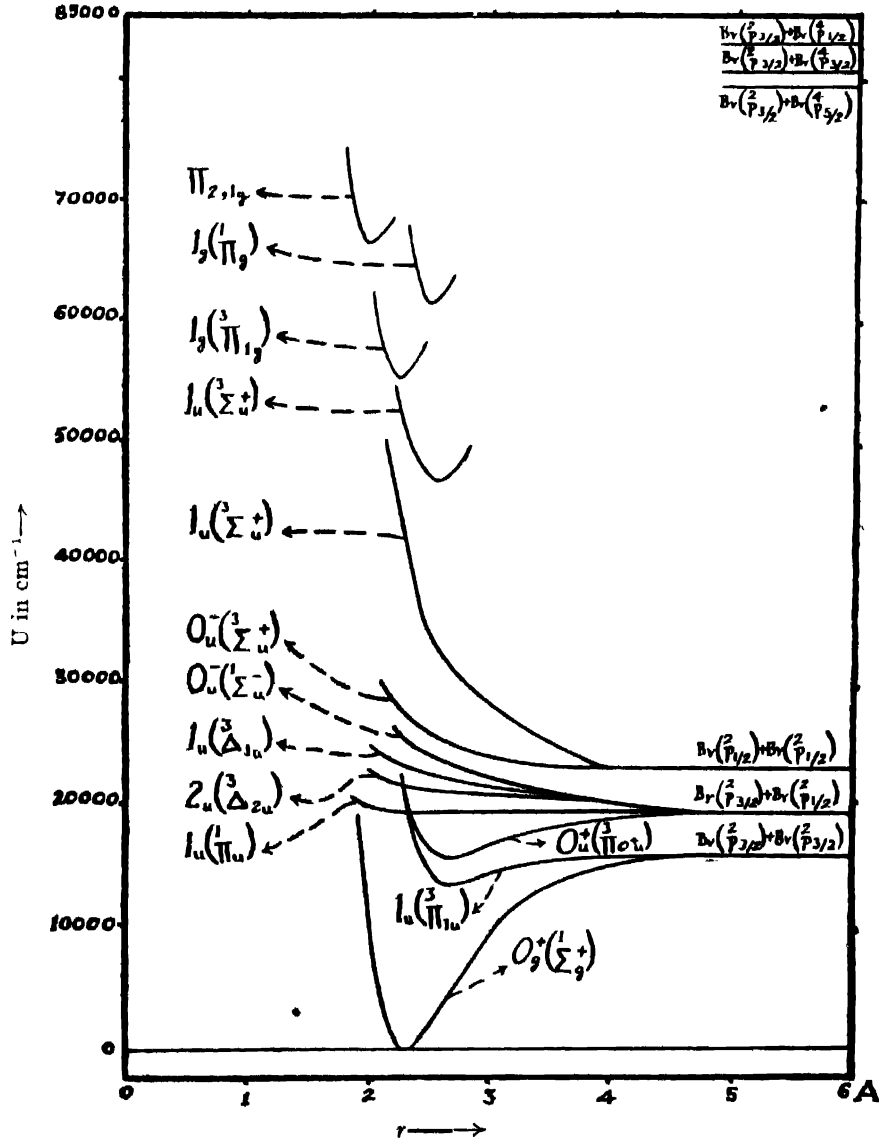

FIG. 2

Potential energy curves for Br_2 molecule

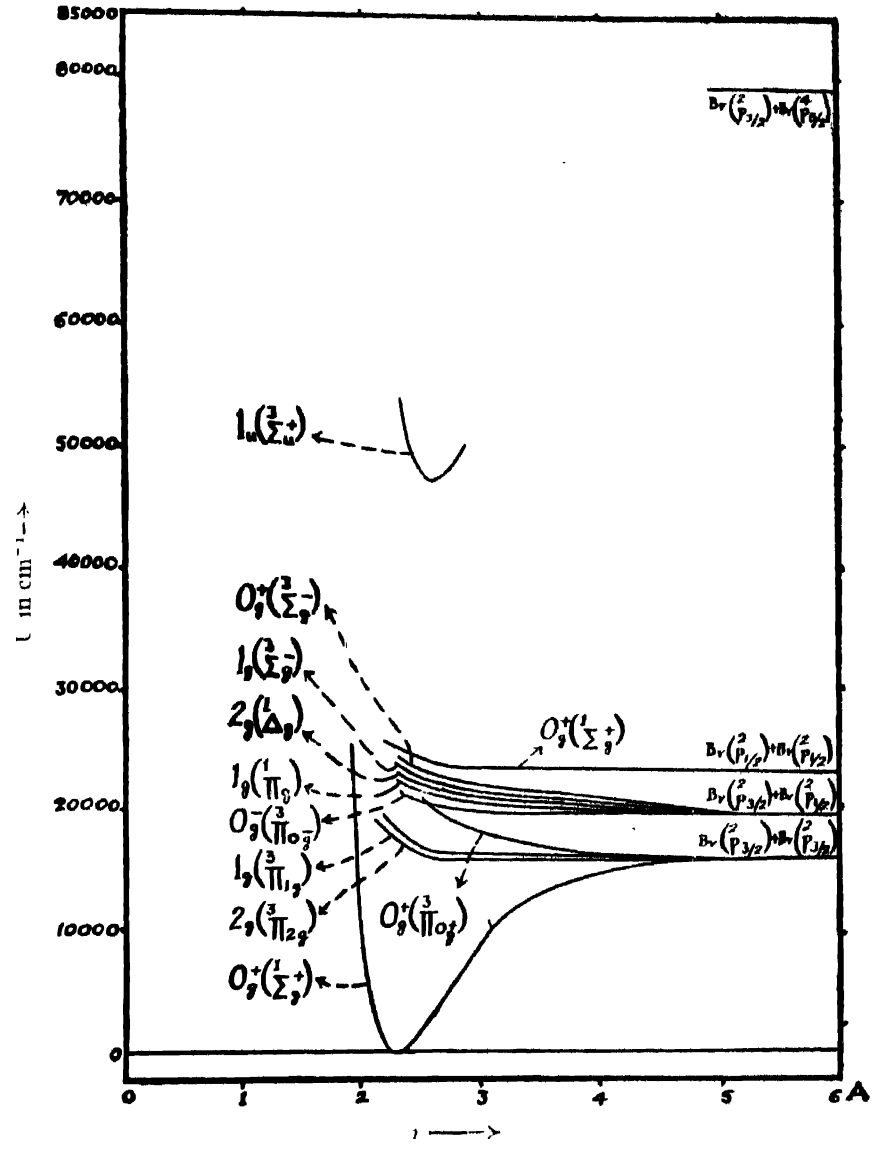

FIG. 3

Potential energy curves for Br_2 molecule

6700-5000A consists of bands degraded towards red. According to Uchida and Ota, these bands occur in two systems which arise from two different initial states having frequencies of 192 and 151 cm^{-1} to a common final level which is different from the ground state and which has a frequency of about 360 cm^{-1}. Unlike in iodine, therefore, these emission bands do not coincide with absorption bands. This fact is confirmed from the spectra taken for absorption and emission on a 3-prism glass Steinheil spectrograph Uchida and Ota indicate also the probability that the discrete emission bands may not be due to the neutral bromine molecule.

The second division from 4250 to 2000A consists of diffuse bands (Paper IV) which like those in iodine occur in groups, the difference being that the constituent bands in different groups in bromine overlap one another. In general, these groups appear as continua superposed by different maxima whereas the constituent bands of different groups in iodine are well separated and appear like sequences.

These groups also can be explained as arising in stable levels, and having repulsive states for their final levels. The various stable states are $1_u(^3\Sigma_u^+)$ at 47000 cm^{-1} and $1_g(^3\Pi_{1g})$, $1_g(^1\Pi_g)$ and $\Pi_{2,1g}$ with frequencies 330, 220 and 480 cm^{-1} respectively at 55534, 61444 and 66500 cm^{-1}. Of these four states only $1_u(^3\Sigma_u^+)$ at 47000 cm^{-1} can combine with the ground state $O_g^+(^1\Sigma_g^+)$ and so we expect in the extreme quartz ultraviolet, absorption bands in bromine corresponding to P-R, K-M bands in iodine. In fact Aickin and Bayliss (1938) have indicated the presence of a weak band system accompanying the continuous absorption in the ultraviolet. As can be seen from the potential energy curves of bromine molecule (Fig. 2) the repulsive curve $\sigma_g^2, \pi_u^3, \pi_g^3, \sigma_u^2$. $1_u(^3\Sigma_u^+)$ and the stable curve $1_u(^3\Sigma_u^+)$ at 47000 cm^{-1} arising from the configuration $\sigma_g, \pi_u^4, \pi_g^4, \sigma_u$, run close together on the left hand side. So it is likely that the band absorption will be so overlapped by strong continuous absorption as not to be observed easily. Besides the four stable states observed in bromine, there is a fifth state $O_u^+(^1\Sigma_u^+)$ occurring in absorption and emission in iodine. Probably the corresponding bands of bromine arising in $O_u^+(^1\Sigma_u^+)$ lie in the vacuum ultraviolet region.

There are five groups arising in $1_g(^3\Pi_{1g})$ with an average wavenumber separation of about 330 cm^{-1} among the constituent bands which represents the vibrational frequency of the initial state. These groups have for their final levels the repulsive states $O_u^-(^3\Sigma_u^-)$, $O_u^-(^1\Sigma_u^-)$, $1_u(^3\Delta_{1u})$, $2_u(^3\Delta_{2u})$ and $1_u(^1\Pi_u)$ of which the first dissociates into $Br(^2P_{\frac{1}{2}}) + Br(^2P_{\frac{1}{2}})$ atoms at 23266 cm^{-1} and the remaining into $Br(^2P_{\frac{3}{2}}) + Br(^2P_{\frac{1}{2}})$ at 19581 cm^{-1}. The $1_g(^1\Pi_g)$ state at 61444 cm^{-1} forms the initial level of four groups of bands with a wavenumber separation of 220 cm^{-1} among the constituent bands, (which represents the ω value of the initial state) and of a broad band at 20230 cm^{-1}. The final states of the four groups are the same as those of the second to fifth groups arising in $1_g(^1\Pi_{1g})$ and the broad band has for its final level, $1_u(^3\Sigma_u^+)$ dissociating into $Br(^2P_{\frac{1}{2}}) + Br(^2P_{\frac{1}{2}})$ atoms, (*vide* Figs. 2, 3).

The $\Pi_{2,1g}$ state at 66500 cm^{-1} forms the initial level of the two groups of bands in the extreme ultraviolet region which have a wavenumber separation of about 480 cm^{-1} which roughly represents the vibrational frequency of the initial state. The final levels of these groups are the same as those of the last two groups arising in $1_g(^3\Pi_{1g})$ state.

Finally the state $1_u(^3\Sigma_u^+)$ at 47000 cm^{-1} forms the initial level for nine broad bands which are too broad and irregularly separated from one another

to be regarded as a single group. These nine bands have for their final levels the following repulsive states: O_u^+ ($^1\Sigma_u^+$), O_u^- ($^3\Sigma_u^-$), 1_u ($^3\Sigma_u^-$), 2_g ($^1\Delta_g$), 1_g ($^1\Pi_g$), O_g^- ($^3\Pi_{0g^-}$), O_g^+ ($^3\Pi_{0g^+}$), 1_g ($^3\Pi_{1g}$) and 2_g ($^3\Pi_{2g}$). Of these the first dissociates into $Br(^2P_{\frac{1}{2}}) + Br(^2P_{\frac{1}{2}})$ atoms. The five states from second to sixth, dissociate into $Br(^2P_{\frac{3}{2}}) + Br(^2P_{\frac{1}{2}})$ and the last three into $Br(^2P_{\frac{3}{2}}) + Br(^2P_{\frac{3}{2}})$. It should be noted that the transitions from the stable state to the second, third and fourth repulsive states will not be possible if there is case (*a*) or (*b*) type coupling, because of $\Sigma^+ \leftarrow\!\!\!\!\!\!\rightarrow$ and $\Sigma \leftarrow\!\!\!\!\!\!\rightarrow \Delta$ rules and they will be possible only if there is case (*c*) type coupling. The existence of these transitions which alone explains the experimental data is a proof of the existence of the case (*c*) type coupling in these states of bromine molecule as in iodine where Ω becomes a good quantum number and Λ and Σ lose their significance.

(3) *Chlorine.*—The spectrum of chlorine, similarly to that of iodine and bromine can also be divided into two divisions (Paper V). The first division in the region 5000 to 3000A consists of discrete bands degraded towards red, only part of which have been analysed by Cameron and Elliot as due to Cl_2^+ (19,37-38-30). The discrete emission bands, like those of bromine do not coincide with absorption bands. The second division in the region 3063-1850A consists of continuous bands which can be divided easily into three sets. Paper V deals with these bands. These three sets of continua arise in three different stable states 1_u ($^3\Sigma_u$), 1_u ($^3\Pi_{1u}$) and 1_g ($^1\Pi_g$) at 58000, 67700 and 75000 cm^{-1} respectively. The bands due to the state Π_2, 1_u which occur in bromine and iodine and those due to O_u^+ ($^1\Sigma_u^+$) which occur in iodine will probably lie in the vacuum region in chlorine.

The first set consisting of six continua between 3063-2715A will arise in 1_u ($^3\Sigma_u^+$) and will have for their final levels the following repulsive states: O_g^+ ($^1\Sigma_g^+$), O_g^- ($^3\Sigma_g^-$), 1_u ($^3\Sigma_u^-$), 2_g ($^1\Delta_g$), 1_g ($^1\Pi_g$), O_g^- ($^3\Pi_{0g^-}$) of which the first dissociates into $Cl(^2P_{\frac{1}{2}}) + Cl(^2P_{\frac{1}{2}})$ atoms at 21784 cm^{-1} and the remaining into $Cl(^2P_{\frac{3}{2}}) + Cl(^2P_{\frac{1}{2}})$ at 20903 cm^{-1}. It should be mentioned that these six states can combine with 1_u ($^3\Sigma_u^+$) if there is case (*c*) type coupling. If the coupling is akin to case (*a*) type, transitions from 1_u ($^3\Sigma_u^+$) to the second, third and fourth states will not be possible because of $\Sigma^+ \leftarrow\!\!\!\!\!\!\rightarrow \Sigma^-$ and $\Sigma \leftarrow\!\!\!\!\!\!\rightarrow \Delta$ rules. The six continua can, however, be explained according to case (*a*) type coupling as due to transitions from the stable state $^3\Sigma_u^+$ to the repulsive states $^1\Sigma^+$, $^1\Pi_g$, $^3\Pi_{0g^-}$, $^3\Pi_{0^-}$, $^3\Pi_{1g}$, and $^3\Pi_{2g}$ of which the first dissociates into two $Cl(^2P_{\frac{1}{2}})$ atoms, second and third into $Cl(^2P_{\frac{3}{2}}) + Cl(^2P_{\frac{1}{2}})$ atoms and the remaining two into two $Cl(^2P_{\frac{3}{2}})$ atoms at 20922 cm^{-1}.

1_g ($^3\Pi_{1g}$) at 67700 cm^{-1} forms the initial level of the seven continuous bands in the second set from 2565 to 2097A which have for their final levels the following repulsive states: O_u^- ($^1\Sigma_u^-$), 1_u ($^3\Delta_{1u}$), 2_u ($^3\Delta_{2u}$), 1_u ($^1\Pi_u$),

O_u^- ($^3\Pi_{0-}$), 1_u ($^3\Pi_{1u}$) and 2_u ($^3\Pi_{2u}$) of which the first four dissociate into Cl ($^2P_{\frac{3}{2}}$) + Cl ($^2P_{\frac{1}{2}}$) and the remaining three into Cl ($^2P_{\frac{3}{2}}$) + Cl ($^2P_{\frac{3}{2}}$) atoms. 1_u ($^1\Pi_u$) forms the initial state of the three continua in the third set from 1997 to 1855Å which have their final levels the same as those of the first three bands of the second set. (*Vide* Figs. 4 and 5).

(4) *General Remarks.*—Taking the experimental results in the three spectra we come to the following conclusions: (*a*) the emission spectra of

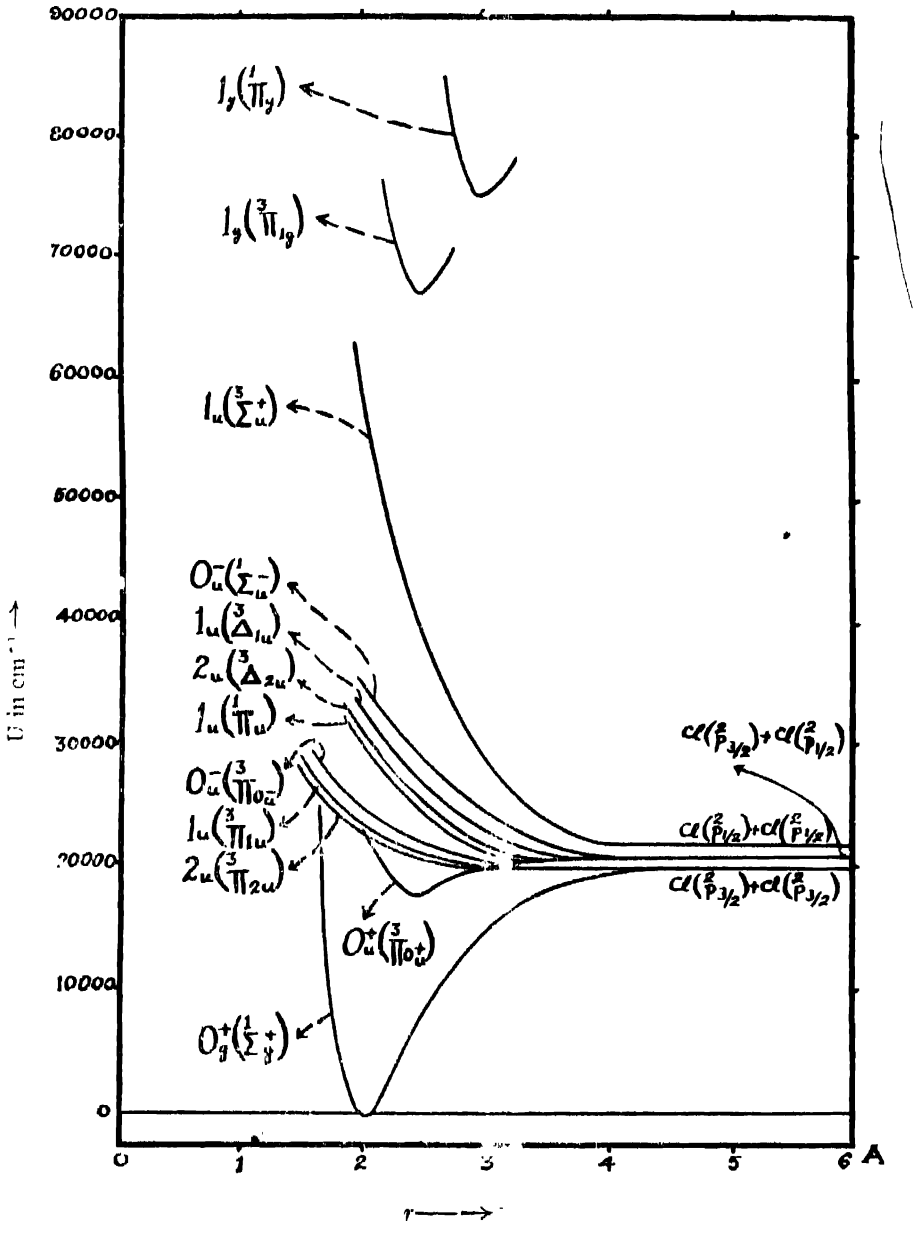

FIG. 4

Potential energy curves for Cl_2

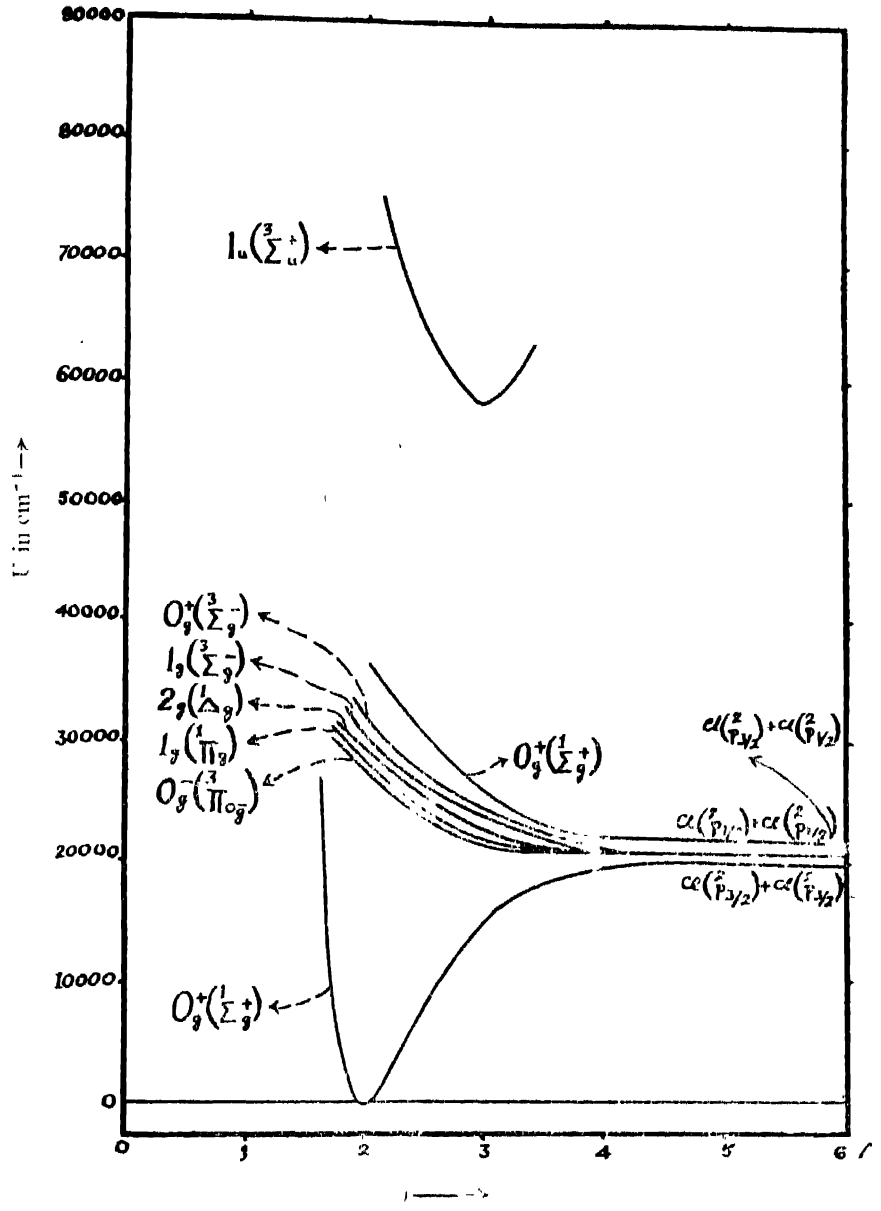

FIG. 5

Potential energy curves for Cl_2 molecule

these three molecules can be divided broadly into two divisions ; the first (visible region) consists of discrete bands degraded towards red, the origin of the bands being, however, different in the three cases. The second division consists of diffuse bands. (*b*) The three spectra apparently appear to be similar though the chlorine spectrum is displaced towards shorter wavelengths compared to that of bromine and the spectrum of bromine to that of iodine. (*c*) One striking difference in these three spectra is that the constituent bands in different groups in general are well separated from one another in iodine

and appear like sequences ; whereas in bromine they merge into one another and in fact the different groups of bromine generally appear as continua superposed by different maxima. This tendency appears to have been developed still further in chlorine where we get only broad continuous bands. (d) All the bands in the second division in the three molecules can be explained as arising in different stable states and having various repulsive states for their final levels. The difference in the nature of the diffuse bands in the three spectra can be well explained as due to the following nature of the repulsive states. Mostly the repulsive states in iodine are nearly flat and so the bands in every group due to transitions from different vibrational levels of the initial stable state to the flat potential energy curve are well separated from one another by wavenumber differences which represent the spacings of the vibrational levels in the initial state. In bromine the repulsive states are slightly steep and so different bands in every group overlap one another. Finally in chlorine the repulsive curves are still more steep and therefore, we get only broad continua.

(B) ABSORPTION SPECTRA

(1) *Iodine* : Iodine has absorption bands in the near infra-red region from 8375-9300A. They are due to a transition from the ground state $\sigma_g^2, \pi_u^4, \pi_g^4, O_u^+ ({}^1\Sigma_g^+)$ having a frequency of 214 cm^{-1} to a state $\sigma_g^2, \pi_u^4, \pi_g^3, \sigma_u$. 1_u $({}^3\Pi_{1u})$ at 11803 cm^{-1} with $\omega = 44$ cm^{-1}. There is a continuous maximum at 7370A observed by Brown (1931) which is due to a transition from the ground state to the repulsive part of 1_u $({}^3\Pi_{1u})$ state. There are also bands in the visible region, which converge to a limit at about 4995A followed by continuous absorption. The absorption curve has a maximum at 5200A according to Rabinowitch and Wood (1936). These bands together with the continuum are due to a transition from the ground state to $\sigma_g^2, \pi_u^4, \pi_g^3, \sigma_u$; $O_u^+ ({}^3\Pi_{0u})$ at 15508 cm^{-1} with $\omega = 128$ cm^{-1}. Besides the bands in the visible and infrared, iodine shows absorption bands in the quartz ultraviolet and fluorite regions. Bands in the quartz ultraviolet region 2150-1950A are measured by Kimura and Miyanishi (K-M) and those from 2760 to 2090A by Pringsheim and Rosen (P-R). They have analysed these bands but a more satisfactory analysis is given by Sponer and Watson (1929). The analysis of Sponer and Watson is, however, not complete and does not include all the bands of Pringsheim and Rosen.

A complete review of the experimental work on absorption in the quartz ultraviolet is given in Paper VII. The analysis proposed there includes all the bands in the quartz ultraviolet (P-R, K-M bands). From this analysis it has been shown that the bands from 2760 to 1950A are due to a transition from the ground state to a state σ_g, π_u^4, π_g^4, σ_u. 1_u $({}^3\Sigma_u^+)$ at 44900 cm^{-1} and with $\omega = 90$ cm^{-1}. The convergence limit of these bands by extrapolation comes out as 58000 ± 1000 cm^{-1}.